

Modeling and energy management of hangar thermo-electrical microgrid for electric plane charging considering multiple zones and resources[☆]

Pablo Verdugo, Claudio Cañizares, Mehrdad Pirnia^{*}

University of Waterloo, 200 University Ave. West, Waterloo, N2L 3G1, Ontario, Canada

ARTICLE INFO

Keywords:

Airport microgrid
Battery degradation
E-plane charging
Hangar thermal model
Heat pumps
Solar PV

ABSTRACT

Achieving net zero goals by 2050 is driving an energy transition towards clean electrical energy. Consequently, many initiatives have been proposed aiming to reduce carbon emissions in the building and transportation sectors, focusing, for instance, on the implementation of efficient heating and cooling systems based on heat pumps and the use of electric planes. Microgrids can effectively integrate thermal and electrical energy resources and loads to satisfy customer demands while providing technical, economic, and environmental benefits. Thus, this paper proposes the implementation of a model of a hangar microgrid and its Energy Management System to optimize the dispatch of resources of such thermo-electrical airport grid, using a Model Predictive Control approach to address uncertainties, and including a detailed building thermal model, heat pump modeling for the heating and cooling systems, and battery degradation. The proposed mathematical model of the Energy Management System is applied to a model of a microgrid being developed for a hangar at the Waterloo Wellington Flight Centre in Ontario, Canada, taking into account the specific characteristics of the microgrid's components, the expected energy consumption of the equipment and the electric plane used for pilot training based on field measurements, and multi-room temperature control requirements, seeking to ensure a reliable and cost-effective operation, while considering the occupants' comfort in different spaces. The results indicate that the proposed Energy Management System model, featuring multi-room temperature control through multiple thermal resources, can achieve significant savings in operational costs and CO₂ emissions compared to a scenario where the microgrid is not deployed and another where a single-room building thermal model with a single heat pump is included.

1. Introduction

Many initiatives across the world are being pursued to address climate change and facilitate a transition toward a low-carbon economy to achieve a Net Zero 2050. This includes the integration of clean energy generation sources and the electrification of thermal and transportation energy systems. In this context, a significant increase in the use of electricity for space heating is required to achieve net zero in the buildings sector, especially in Canada [1]. However, keeping electricity affordable and reliable, and addressing peak demand issues present a challenge for electric utilities. Hence, there is a significant drive to the implementation of energy-efficient buildings using Heat Pumps (HPs) to help achieve these objectives.

The 184 member states of the International Civil Aviation Organization (ICAO) adopted in 2022 a long-term global aspirational goal of net zero carbon emissions from international aviation by 2050 [2]. Therefore, the Government of Canada and the aviation industry have developed Canada's Aviation Climate Action Plan [3], with Canadian airports

investing thus far over \$14 billion in capital infrastructure and improvements, including the use of Renewable Energy Sources (RESs) for electricity generation, and Electric Vehicles (EVs) and Electric Planes (E-Planes) for transportation.

Microgrids can effectively integrate thermal and electrical energy resources and loads to satisfy customers' demand and improve overall efficiency. Thus, the Energy Management System (EMS) of microgrids should be capable of controlling both electric and thermal systems to ensure a reliable and cost-effective operation. In this context, the energy management of thermo-electrical microgrids is a challenging task, since several aspects need to be considered for their operation, such as adequate modeling of the microgrid components considering computational burden, the incorporation of thermal comfort through proper temperature settings, and the variability of RES, energy demand, and environmental conditions. Researchers have identified the benefits of combining the supply and demand of electrical and thermal energy

[☆] The editing of this document was supported by ChatGPT, OpenAI, <https://chat.openai.com/chat>.

^{*} Corresponding author.

E-mail addresses: pverdugo@uwaterloo.ca (P. Verdugo), ccanizar@uwaterloo.ca (C. Cañizares), mpirnia@uwaterloo.ca (M. Pirnia).

Nomenclature	
Acronyms	
BESS	Battery Energy Storage System
COP	Coefficient of Performance
DER	Distributed Energy Resource
DG	Distributed Generation
DOD	Depth of Discharge
EH	Electric Heater
EMS	Energy Management System
ESS	Energy Storage System
EV	Electric Vehicle
GHG	Green-House Gas
HP	Heat Pump
HVAC	Heating Ventilation and Air Conditioning
MPC	Model Predictive Control
PV	Photo-Voltaic
RES	Renewable Energy Source
SOC	State of Charge
TEC	Thermal Equivalent Circuit
TES	Thermal Energy System
TOU	Time of Use
WWFC	Waterloo Wellington Flight Centre
Sets and Indices	
min, max	Minimum and maximum limits
{ <i>nc</i> }	Rooms with no temperature control
{ <i>ng</i> }	Rooms not at ground level
{ <i>ph</i> }	Planes' hangar room
<i>f</i> ∈ <i>F</i>	Floors of building
<i>h</i> ∈ <i>H</i>	Heat pumps (HPs)
<i>i, j</i> ∈ <i>R</i>	Rooms
<i>k</i> ∈ <i>T</i>	Time steps
<i>l</i> ∈ <i>L</i>	Partitions for battery degradation model
<i>n</i> ∈ <i>N</i>	Batteries
<i>s</i> ∈ <i>S</i>	Surfaces of building envelope
<i>w</i> ∈ <i>W</i>	Internal walls of building
Parameters	
Δt_k	Time interval between step <i>k</i> and step <i>k</i> + 1 [h]
$\eta_n^{ch}, \eta_n^{dch}$	Battery charging/discharging efficiency
μ_i	Thermal distribution factor for room <i>i</i>
$\phi_{n,l}$	Piece-wise linear degradation coefficient
$\psi_h^{HP_c}$	HP cooling efficiency reduction coefficient
$\psi_h^{HP_h}$	HP heating efficiency reduction coefficient
ρ^{air}	Air density [kg/m ³]
σ_i^s	Shading coefficient of building surface <i>s</i>
τ_i^s	Transmission coefficient of windows
Vol_i	Volume for room <i>i</i> [m ³]
θ^{gr}	Ground temperature [K]
$\theta_h^{HP,out}$	HP outlet temperature [K]

in thermo-electrical microgrids. However, limitations can be identified in the existing literature. For instance, several authors have considered the thermal demand as an input parameter to the EMS [4–10]. Other

θ_k^{ext}	Ambient temperature [K]
ξ_i^s	Amount of windows on building surface <i>s</i>
A_i^f, A_i^s	Area of building floor/surface [m ²]
A_{ij}^w	Area of internal wall between room <i>i</i> and <i>j</i> [m ²]
c^{air}	Air specific heat [kJ/(kgK)]
c_k^{em}	Cost of CO2 emissions [\$/kWh]
c_k^{gp}	Cost of electricity from the grid [\$/kWh]
C_i^{in}	Thermal capacity of room <i>i</i> [kJ/K]
$I_{i,k}$	Solar irradiation [kW/m ²]
P^{EH}	EH active power [kW]
P_k^{bd}	Active power building demand [kW]
P_k^{ep}	Active power e-plane demand [kW]
P_k^{PV}	PV plant output [kW]
U	Thermal transmittance [kW/(m ² K)]
v_k^{rate}	Ventilation rate [1/h]
Variables	
$\Phi_{n,l,k}$	Piece-wise linear degradation function
$\theta_{i,k}^{in}$	Indoor temperature in room <i>i</i> [K]
P_k^{gp}	Active power from electric grid [kW]
$P_{h,k}^{HP}$	HP input active power [kW]
$P_{n,l,k}^{ch}$	Battery charging power [kW]
$P_{n,l,k}^{dch}$	Battery discharging power [kW]
$Q_{h,k}^{HP_c}$	HP cooling thermal power [kW]
$Q_{h,k}^{HP_h}$	HP heating thermal power [kW]
$Q_{i,k}^{env}$	Heat transfer through building envelope [kW]
$Q_{i,k}^{gr}$	Heat transfer with the ground [kW]
$Q_{i,k}^{ig}$	Internal heat gains [kW]
$Q_{i,k}^{sun}$	Thermal solar power through windows [kW]
$Q_{i,k}^{vent}$	Heat transfer due to ventilation [kW]
$Q_{ij,k}^{trf}$	Thermal power transferred between rooms [kW]
$SOC_{n,l,k}$	Battery State of Charge (SOC) [kWh]
u_k	ON/OFF state of EH (1=ON)
$v_{h,k}$	HP heating/cooling decision (1=heating, 0=cooling)
$y_{n,l,k}$	Battery charge/discharge decision (1=charge, 0=discharge)
z	EMS objective function [€]

works incorporate a building thermal model to account for temperature control, considering the building as a single structure such as in the case of [11], where a multi-agent-based EMS is proposed for coordinated energy and comfort management in integrated buildings and a microgrid system. Ref. [12] studies a distributed EMS for community microgrids for optimizing the dispatch of Distributed Energy Resources (DERs), storage systems and home appliances. Similarly, [13] presents a Model Predictive Control (MPC)-based EMS for an isolated microgrid with thermal resources, and [14] adopts a nonlinear formulation to capture the nonlinear thermal models response in an MPC-based EMS. Finally, [15] focuses on price-based demand response and indoor temperature control to flexibilize the electric and thermal loads, while [16] proposes various control strategies for the operation of residential EMSs considering variable-speed HPs, with a practical application in a typical Greek single-family house using a one-room building model.

The application of techniques for including thermal comfort in energy management models without building thermal models is discussed in [17], using a linear thermal dynamic model in a data-driven approach to forecast Photo-Voltaic (PV) generation, demand and room thermal dynamics to schedule the dispatch of Heating, Ventilation, and Air Conditioning (HVAC) systems. Ref. [18] uses a comfort reward function to evaluate the deviation of residential room temperatures from a predetermined comfort temperature in a building model-free approach, and in [19], a deep neural network-based approach for predicting occupants' thermal comfort is presented.

Although extensive work has been carried out on the energy management of thermo-electrical microgrids, research on the incorporation of models that allow detailed representation of different rooms in a building with independent HVAC systems is limited. For example, [20] investigates the use of pre-cooling strategies in residential households to mitigate the duck-curve effects using multi-room building thermal models with a single HVAC system. Ref. [21] proposes a novel Price Storage Control (PSC) strategy that considers thermal satisfaction, available thermal storage, and energy prices to determine the dispatch of a single HP using a multi-room building model, while not considering the incorporation of DERs. Similarly, [22] focuses on the study of thermal dynamic operations of passive buildings and model parameter identification with only one HVAC system, which does allow for independent temperature control. Thus, for buildings with multiple HVAC systems requiring independent room temperature controls, the modeling of heat transfer dynamics between rooms is required, as these significantly influence the dispatch of thermal resources.

Due to the need to transition to a clean-energy environment that includes aviation systems, research on the development of airport clean-energy microgrids is increasing. In this context, [23] considers the loads of an airport cargo terminal microgrid for the application of an Energy, Economic, and Environmental (3E) performance assessment. The work in [24] focuses on smart charging and flight schedule optimization of hybrid electric aircraft. Airport electric ground support equipment has also been studied to achieve optimal fleet scheduling [25], and for providing ancillary services to the grid [26]. Another application for ancillary services is discussed in [27], where researchers propose the concept of Aviation-to-Grid (A2G) using the electric aircraft charging system to provide primary and secondary frequency response to the grid. Planning and design of airport microgrid infrastructure is studied in [28] to accommodate EVs and electric aircraft, and [29] discusses the optimal capacity of PV generation and Battery Energy Storage Systems (BESSs) in such microgrids. Aiming at the same goal, the study in [30] focuses on the benefits produced from incorporating PV and various BESS dispatch scenarios considering the increasing power demands from electric aircraft and EV charging in a Swedish airport. Furthermore, the operation of different airport microgrid components is presented in [31], which integrates the use of hydrogen fuel cells, as well as in [32], which expands the findings of [31] within a resilience assessment context.

In most of the existing literature, there is a predominant focus on determining the optimal sizing of microgrid components or optimizing the schedule and operations of airport fleets, namely, ground support equipment and electric aircraft, neglecting the aspects related to the operation of airport buildings and their electrical and thermal energy demands. Thus, this paper proposes the implementation of an MPC-based EMS model for an airport hangar thermo-electrical microgrid, capable of determining the optimal dispatch of its resources while ensuring occupants' comfort through predefined temperature settings in various rooms, including a detailed building model to account for heat exchange between rooms. Furthermore, the EMS model includes the representation of BESS degradation considering the Depth of Discharge (DOD) of the battery and e-plane charging requirements. Hence, the main contributions of this paper are as follows:

- Proposing an EMS for a detailed model of a hangar microgrid including DERs, such as Solar PV and BESS, and e-plane charging.
- Implementing a detailed hangar thermal model considering accurate representation of multiple rooms and the associated temperature control requirements, and the independent dispatch of thermal resources such as HPs and Electric Heaters (EHs) for temperature control in each hangar room considering heat exchanges between zones.
- Applying the proposed EMS to the model of an actual microgrid being deployed at Waterloo Wellington Flight Centre (WWFC) Hangar 7 in Ontario, Canada, with a detailed representation of its components, to demonstrate the advantages of the proposed microgrid model and operation through model and cost comparisons.

The rest of the paper is organized as follows: Section 2 provides a background overview of the concepts related to microgrid EMS, using MPC to address uncertainties, and the modeling of thermal systems and battery degradation. Section 3 describes an optimization model for a microgrid EMS, incorporating thermal and electric systems including RES and BESS, a detailed building model to account for different thermal contribution sources and heat exchanges, and the modeling of HPs for the provision of heating and cooling in multiple rooms. Section 4 comprises a practical application to an existing hangar building with a grid-connected microgrid being deployed for the WWFC, with flight simulators, and HP-based HVAC systems, considering e-plane charging demand and the various thermal needs of the building for different electricity tariffs. Modeling and operating cost comparisons are also presented in this section to showcase the advantages of the proposed microgrid models and operation. Finally, the summary and the conclusions of these studies are presented in Section 5.

2. Background

2.1. Microgrid energy management systems

A microgrid is defined as a cluster of controllable and uncontrollable loads, and DERs, which comprise Distributed Generation (DG), Energy Storage Systems (ESSs), and RESs, operated in coordination to reliably supply electricity [33]. The EMS is at the core of secondary control in microgrids for both grid-connected and stand-alone operating modes, and can be either centralized or decentralized. In a centralized EMS, which is the focus of this paper, a central controller determines the dispatch of the resources to achieve the predefined objectives based on the information obtained from forecasting systems.

Given the unpredictable nature of renewable resources and demand, the EMS should consider these uncertainties to control the power exchanged among microgrid's components, ensuring reliable and economical operation by the optimal commitment and dispatch of the variable DERs for both grid-connected and isolated operating modes [33]. The MPC approach has been broadly used to address in practice uncertainties in EMS [13,33,34]. One of the principles within the MPC framework is a rolling horizon control, which is an optimization-based control strategy where at each time step k , the horizon moves forward with the optimization control problem, with fixed constraints being solved continuously. The states of the system at future time steps are calculated as a function of the control variables and initial system conditions, while the optimization problem calculates a control sequence for the entire horizon such that the selected objective function is minimized, but only the control action for the next time step is implemented. In an MPC-based EMS, the optimization problem is solved at each time step over a chosen time horizon T given the forecasts of uncertain inputs, in order to calculate the set points for the generation power accounting for the most likely value of those inputs. The time intervals can have either uniform or non-uniform durations, providing flexibility in the computational complexity of the model [13].

2.2. Building thermal model

To accurately represent the thermodynamic aspects of loads, the Thermal Equivalent Circuit (TEC) method is employed to model Thermal Energy Systems (TESS) in EMS, which is based on an analogy between thermal and electrical variables to represent heat transfer processes using an electrical circuit with lumped parameters [35]. The equivalent circuit can then be solved by using electric circuit techniques to derive the differential equations that describe the thermodynamic processes. In this context, the thermal capacitance C of a material can be formulated as follows:

$$C = c^p \rho V ol \quad (1)$$

where, for a particular material, c^p represents the specific heat, ρ defines the density, and $V ol$ represents the volume.

The building thermal model shown in Fig. 1 is used to derive the constraints for the EMS related to thermal dynamics. Hence, as per [13,20], a simpler first-order model can effectively capture the dynamics of the indoor air temperature and account for the main heat gains in each room i , as follows:

$$C_i^{in} \frac{d\theta_i^{in}}{dt} = \mu_i Q_h^{HP} - Q_{ij}^{rf} - Q_i^{env} - Q_i^{gr} + Q_i^{sun} + Q_i^{ig} \quad (2)$$

$$C_i^{in} \frac{d\theta_i^{in}}{dt} = \mu_i Q_h^{HP} - \sum_{j \in \mathcal{R}} \frac{\theta_i^{in} - \theta_j^{in}}{R_{ij}^w} - \frac{\theta_i^{in} - \theta^{ext}}{R_i^s} - \frac{\theta_i^{in} - \theta^{gr}}{R_i^f} + Q_i^{sun} + Q_i^{ig} \quad (3)$$

where C_i^{in} , which is the thermal capacitance that defines the indoor temperature dynamics in each room, depends on the thermal power contribution from HPs Q_h^{HP} associated with the thermal distribution factor μ_i for each room; the heat transfer between room i and room j Q_{ij}^{rf} ; the heat transfer through the building envelope Q_i^{env} ; the heat transfer between each room and the ground Q_i^{gr} ; the thermal power due to solar irradiation entering through the windows Q_i^{sun} ; and the internal heat gains defined for each room Q_i^{ig} considering sensible heat from people, as per [36], and lighting and equipment, based on [37]. Furthermore, R_i^s , R_{ij}^w , and R_i^f denote the thermal resistance of the material between two adjacent areas, i.e., the outside walls, the internal walls between rooms, and the floors, respectively. Note that (2) is discretized in the EMS model using a time step in the order of minutes. All variables and parameters in these and other equations are defined in the Nomenclature, together with their units, except for those that are dimensionless.

The thermal model used considers the walls, floors, and ceiling through thermal conductivities, but their thermal storage properties are not directly considered. Since the thermal conductivities of partition walls are high due to lack of insulation, their energy storage capabilities are low. On the other hand, other insulated surfaces have low conductivity and hence have the potential to store energy. The thermal capacitance of these surfaces is typically lumped in the rooms' thermal capacitances to decrease the number of variables in the model and thus simplify the building model to maintain computational efficiency, while reducing modeling errors by indirectly accounting for these relevant storage elements.

2.3. Battery degradation model

Microgrids with high penetration of RES can significantly benefit from the use of BESS in terms of stability, reliability, and performance. However, microgrid EMS applications have typically overlooked issues related to battery degradation, despite the significant impact that BESS operation can have on battery life in the long term, making degradation a relevant aspect of an EMS [34]. BESS degradation can be attributed to two factors, namely, calendar aging and cycle aging. Cycle aging is a function of the number of performed cycles and the DOD in each cycle.

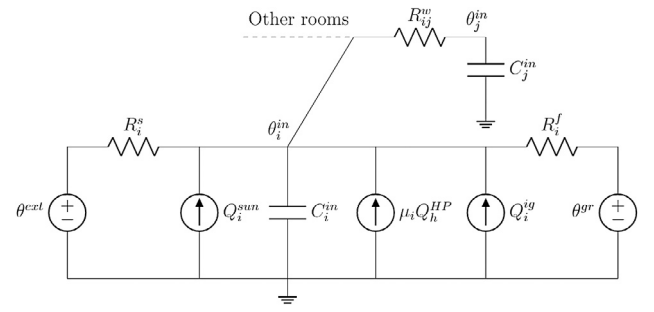


Fig. 1. Thermal circuit of room i [20].

To identify the number of cycles, the Rainflow cycle-counting algorithm has proven to be an effective approach [38]. Since the algorithm does not have an analytical mathematical expression, it cannot be incorporated directly within an optimization problem. Hence, [34] proposes a piece-wise linear representation for which the battery's cycle depth range is split into even partitions $l \in \mathcal{L}$, considering the range of the State of Charge (SOC) in the BESS. Assuming that only half-cycles are identified, the degradation of battery $n \in N$ can then be described as follows:

$$\Phi_{n,l,k} = \frac{\phi_{n,l}}{2} \frac{\Delta t_k}{E_n} \left(P_{n,l,k}^{ch} \eta_n^{ch} + \frac{P_{n,l,k}^{dch}}{\eta_n^{dch}} \right) \quad (4)$$

$$SOC_{n,l,k+1} - SOC_{n,l,k} = \left(P_{n,l,k}^{ch} \eta_n^{ch} - \frac{P_{n,l,k}^{dch}}{\eta_n^{dch}} \right) \Delta t_k \quad (5)$$

$$SOC_{n,l}^{\min} \leq SOC_{n,l,k} \leq SOC_{n,l}^{\max} \quad (6)$$

$$0 \leq P_{n,l,k}^{ch} \leq y_{n,l,k} P_n^{ch,\max} \quad (7)$$

$$0 \leq P_{n,l,k}^{dch} \leq (1 - y_{n,l,k}) P_n^{dch,\max} \quad \forall n \in N, \forall l \in \mathcal{L}, \forall k \in T \quad (8)$$

where (4) denotes the cycle aging function, (5) corresponds to the energy balance in the BESS, (6) represents the SOC limits, and (7) and (8) model the limits for the power that can be stored and supplied by the BESS, respectively. The inclusion of the binary variable $y_{n,l,k}$ in (7) and (8) prevents the simultaneous charging/discharging of the battery. Notably, each battery partition l has its own SOC, which is bounded by the partition's depth range, as per (6). The piece-wise linear degradation coefficient $\phi_{n,l}$ in (4) is obtained from the following cycle depth stress function, derived for lithium-ion batteries [34,38], which is the most popular BESS technology for energy storage applications in microgrids:

$$\Phi_\delta = 5.23 \times 10^{-4} \delta^{2.03} \quad (9)$$

Note that the degradation model considers the DOD δ as the main factor for BESS degradation, neglecting temperature and average SOC due to their small impact. Furthermore, since grid-scale BESS have capacities greater than fifteen minutes, the effect of current rate on degradation can also be omitted [38].

3. EMS model formulation for hangar microgrids

The EMS model presented in this section aims to optimize the operation of a microgrid that supplies both electricity and heat to a hangar building, considering a detailed representation of the thermal dynamics inside each room. For the electric demand supply, the model considers power from the main grid, PV generation, and BESS operation. The thermal power is assumed to be supplied by air HPs, capable of both heating and cooling, and an EH for the planes' hangar. The occupants' thermal comfort is addressed through the control of the indoor temperature within predefined customer set limits.

The objective function of the EMS model aims to minimize the operating cost of the hangar microgrid as follows, since that is the main objective of deploying microgrids by airport operators:

$$\min z = \sum_{k \in T} (c_k^{gp} P_k^{gp} \Delta t_k) + \sum_{k \in T} \sum_{n \in N} \sum_{l \in \mathcal{L}} E_n RC_n \Phi_{n,l,k} \quad (10)$$

The first term pertains to the cost of electricity from the grid, and the second term represents the costs associated with BESS degradation, where E_n is battery's n capacity, RC_n is the replacement cost, and $\Phi_{n,l,k}$ is the piece-wise linear degradation function obtained from (4). Furthermore, to assess the impact of the microgrid operation on CO2 emissions, a term has been added to the objective function (10), yielding the following objective function:

$$\min z = \sum_{k \in T} (c_k^{gp} P_k^{gp} \Delta t_k) + \sum_{k \in T} \sum_{n \in N} \sum_{l \in \mathcal{L}} E_n RC_n \Phi_{n,l,k} + \sum_{k \in T} (c_k^{em} P_k^{gp} \Delta t_k) \quad (11)$$

where c_k^{em} represents the cost of CO2 emissions associated with the power obtained from the main grid.

The active power balance in the hangar microgrid can be represented as follows:

$$P_k^{gp} + P_k^{PV} + \sum_{n \in N} \sum_{l \in \mathcal{L}} (P_{n,l,k}^{dch} - P_{n,l,k}^{ch}) = P_k^{bd} + P_k^{ep} + \sum_{h \in H} P_{h,k}^{HP} + u_k P^{EH} \quad \forall k \in T \quad (12)$$

where the power from the grid and PV generation, which is the main RES in airport microgrids due to wind generation deployment restrictions, are considered along with the operation of the BESS. Note that P_k^{bd} accounts for the aggregated demand from lighting and electrical equipment in each room, excluding the power consumed by the HPs and the EH. For the latter, u_k is a binary variable that commands the activation of the EH, with a fixed electric power P^{EH} .

The equations that define the thermal dynamics in the microgrid are the following:

$$C_i^{in} \frac{(\theta_{i,k}^{in} - \theta_{i,k-1}^{in})}{3600 \Delta t_k} = \mu_i (Q_{h,k}^{HP_h} - Q_{h,k}^{HP_c}) + Q_{i,k}^{sun} - Q_{i,k}^{env} - \sum_{j \in \mathcal{R}} Q_{ij,k}^{rf} - Q_{i,k}^{vent} + Q_{i,k}^{ig} - Q_{i,k}^{gr} \quad \forall i \in \mathcal{R} \setminus \{ph\}, \forall k \in T \quad (13)$$

$$C_{\{ph\}}^{in} \frac{(\theta_{\{ph\},k}^{in} - \theta_{\{ph\},k-1}^{in})}{3600 \Delta t_k} = u_k P^{EH} + Q_{\{ph\},k}^{sun} - Q_{\{ph\},k}^{env} - Q_{\{ph\},k}^{vent} - \sum_{j \in \mathcal{R}} Q_{\{ph\},j,k}^{rf} + Q_{\{ph\},k}^{ig} - Q_{\{ph\},k}^{gr} \quad \forall k \in T \quad (14)$$

$$Q_{ij,k}^{rf} = \sum_{w \in W} U_{ij}^w A_{ij}^w (\theta_{i,k}^{in} - \theta_{j,k}^{in}) \quad \forall i, j \in \mathcal{R}, \forall k \in T \quad (15)$$

$$Q_{i,k}^{gr} = U_i^f A_i^f (\theta_{i,k}^{in} - \theta^{gr}) \quad \forall i \in \mathcal{R} \setminus \{ng\}, \forall k \in T \quad (16)$$

$$Q_{h,k}^{HP_h} = \psi_h^{HP_h} \frac{\theta_h^{HP,out}}{\theta_h^{HP,out} - \theta_k^{ext}} P_{h,k}^{HP_h} \quad \forall h \in H, \forall k \in T \quad (17)$$

$$Q_{h,k}^{HP_c} = \psi_h^{HP_c} \frac{\theta_h^{HP,out}}{\theta_h^{HP,out} - \theta_k^{ext}} P_{h,k}^{HP_c} \quad \forall h \in H, \forall k \in T \quad (18)$$

$$Q_{i,k}^{sun} = \sum_{s \in \mathcal{S}} \sigma_i^s I_{i,k} A_i^s \tau_i^s \quad \forall i \in \mathcal{R}, \forall k \in T \quad (19)$$

$$Q_{i,k}^{env} = \sum_{s \in \mathcal{S}} U_i^s A_i^s (\theta_{i,k}^{in} - \theta_k^{ext}) \quad \forall i \in \mathcal{R}, \forall k \in T \quad (20)$$

$$Q_{i,k}^{vent} = \frac{v_k^{rate} \rho^{air} V o l_i c^{air} (\theta_{i,k}^{in} - \theta_k^{ext})}{3600} \quad \forall i \in \mathcal{R}, \forall k \in T \quad (21)$$

$$Q_{i,k}^{ig} = N p_{i,k} Q_i^p CLF_k + Q_{i,k}^l + Q_{i,k}^e \quad \forall i \in \mathcal{R}, \forall k \in T \quad (22)$$

In these equations, the thermal dynamics of indoor air are represented by (13), where $Q_{h,k}^{HP_c}$ represents the HP cooling power, as per (3), and ph refers to the planes' hangar. The indoor thermal dynamics

considering the EH modeled in (14), where $u_k P^{EH}$ represents the thermal power contribution of the EH assuming that all the electric power converts to heat. The heat transfer between rooms and between each room and the ground is modeled in (15) and (16), respectively, assuming that the ground temperature remains constant throughout the day, due to the significant thermal mass of the soil and the time horizon of the EMS, and that rooms in the $\{ng\}$ set are not at ground level. The heat and cold provided by the HPs are shown in (17) and (18), respectively. Note that since the efficiency reduction coefficients for heating and cooling are different, the resulting Coefficient of Performance (COP) for each mode of operation is also different, aiming to represent the actual HP operation. Eqs. (19) to (21) represent the thermal power from solar irradiation and the heat transfer through the building envelope and ventilation, respectively. Eq. (22) represents the internal heat gains from building occupants Q_i^p , considering a time-varying cooling factor CLF_k and the number of people in each room $N p_i$ [39], and the heat from lighting $Q_{i,k}^l$ and equipment $Q_{i,k}^e$ in each room.

The operational limits can be considered as follows:

$$\theta_{i,k}^{in,min} \leq \theta_{i,k}^{in} \leq \theta_{i,k}^{in,max} \quad \forall i \in \mathcal{R} \setminus \{nc\}, \forall k \in T \quad (23)$$

$$0 \leq P_{h,k}^{HP_h} \leq v_{h,k} P_h^{HP,max} \quad \forall h \in H, \forall k \in T \quad (24)$$

$$0 \leq P_{h,k}^{HP_c} \leq (1 - v_{h,k}) P_h^{HP,max} \quad \forall h \in H, \forall k \in T \quad (25)$$

where the temperature limits for specific rooms are imposed by (23), and (24) and (25) limit the power consumption of the HP. Observe that the limit for the HP operation for heating and cooling is the same. Furthermore, the binary variable $v_{h,k}$ was included to prevent the simultaneous provision of heating and cooling power.

4. Results and discussion

4.1. Description of the WWFC microgrid components

The WWFC microgrid, illustrated in Fig. 2, comprises a PV system, BESS, four HPs and an EH for indoor temperature control, a building model of WWFC Hangar 7, and a charger for an electric plane. This microgrid will supply energy to the e-plane and the building which has been distributed into ten zones as defined by the system requirements: Electric room (Room 1), restrooms (Room 2), flight simulator 1 (Room 3), flight simulator 2 (Room 4), flight simulator 3 (Room 5), corridor 1 (Room 6), planes' hangar (Room 7), classrooms (Room 8), offices (Room 9), and corridor 2 (Room 10). Based on [37], the room dimensions are portrayed in Table 1 and their thermal characteristics are shown in Table 2, with their geo-position being considered in order to adequately account for the building's thermodynamic aspects. Furthermore, internal heat gains have been modeled by incorporating the expected occupancy in each room shown in Table 3 [40], and the lighting and electrical equipment expected to be installed in the building. Note that the temperature inside each of the flight simulator rooms is controlled independently by a HP, due to the high expected heat gains, and an additional HP is controlling the temperature inside the classroom and providing heating and cooling to the other rooms according to the assigned thermal distribution factors, illustrated in Table 4. As for the planes' hangar, the indoor temperature is controlled by the EMS only through an EH with no direct thermal contribution from the HPs, due to its particular characteristics and use.

The e-plane currently employed for pilot training at the WWFC is powered by batteries connected in parallel with a total nominal capacity of 20 kWh, which are charged through a 20-kW portable charger, connected to a proper power outlet in the planes' hangar [41]. The PV system will have an estimated power output of 30 kW and the microgrid BESS will have a capacity of 20 kWh. Moreover, it is assumed that the main grid is fully capable of supplying the microgrid's power demand. Note that field measurements were considered for

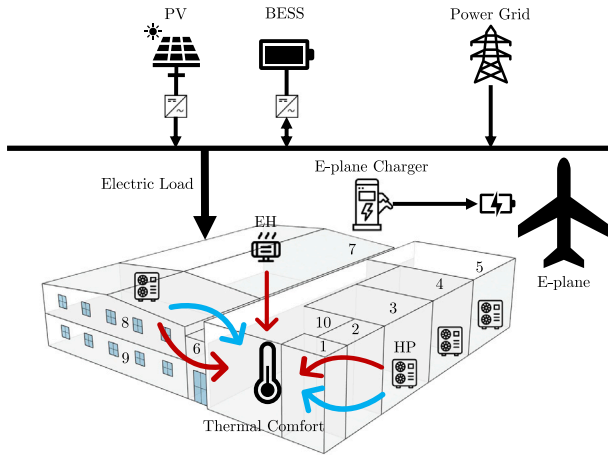


Fig. 2. Microgrid at WWFC Hangar 7, where the blue arrows represent cooling and red arrows represent heating.

Table 1

Room dimensions at WWFC hangar 7 [37].

Room	Area [m ²]	Volume [m ³]
Electric room (Room 1)	6.5	37.3
Restrooms (Room 2)	8.5	48.5
Flight simulator 1 (Room 3)	37.2	213.3
Flight simulator 2 (Room 4)	37.2	213.3
Flight simulator 3 (Room 5)	69.7	400
Corridor 1 (Room 6)	52	222
Planes' hangar (Room 7)	278.7	1444.2
Classrooms (Room 8)	111.5	288.8
Offices (Room 9)	111.5	288.8
Corridor 2 (Room 10)	77.9	447.4

Table 2

Values for thermal parameters in the hangar building [37].

Parameter	Thermal resistance (R) [m ² K/W]
Outside walls in hangar	3.17
Outside walls in new building	4.93
Roof of hangar	3.52
Roof of new building	4.93
Partition walls of corridor	4.93
Partition walls of hangar	3.17
Partition walls of new building	0.25
Slab	1.58
Ground slab	2.38

Table 3

Values for occupant density [40].

Parameter	Value [Persons/m ²]
Classroom	0.65
Laboratories	0.25
Wood/metal shop	0.033
Restrooms	0.043
Office space	0.05

Table 4

Thermal distribution factors.

Parameter	Summer	Winter
μ_1	0	0.07
μ_2	0	0.08
μ_6	0.1	0.1
μ_8	0.3	0.3
μ_9	0.3	0.15
μ_{10}	0.3	0.3

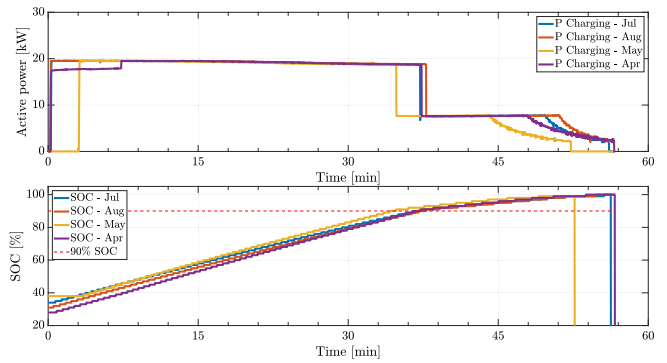


Fig. 3. Measured data representing charging profiles of the e-plane at WWFC for different months.

estimating the power consumption of the flight simulators, since two flight simulators are already in operation allowing for data collection regarding electricity consumption and room temperature. These have yielded approximately 2 kW demand for each flight simulator, with the larger flight simulator expected to require around 4 kW. Thus, significant heat production in the flight simulator rooms is expected, demanding appropriate temperature control mechanisms.

In contrast to other research papers in the context of airport microgrids, where the e-planes power demand is estimated based on flight schedules, this study considers real data to estimate the power of the e-plane charger based on the actual flight operations of the Pipistrel Velis Electro e-plane conducted at the WWFC. Thus, Fig. 3 illustrates the e-plane charging process for different months, as per [42]. Note that, although the ambient temperature has a significant impact on the e-plane charging rate, it is expected that the charging process will take place inside the planes' hangar, where the temperature is always maintained above 10 °C. Moreover, a battery pre-heater has been implemented that uses the existing liquid battery cooling circuit to heat the battery to 20 °C. Thus, the same charging profiles are assumed for Winter and Summer months in terms of power supply.

4.2. Modeling considerations

Airport microgrids must adequately consider the e-plane power demand and constraints in order to optimize operations while minimizing costs. In this regard, based on information gathered from the flight operations of the Pipistrel Velis Electro at WWFC, the e-plane power demand is considered as an input parameter, with predefined flight training schedules subject to environmental conditions and pilot availability. Since one e-plane could perform between five and six training flights per day, and assuming the worst condition in terms of power supply and taking into account the availability of daylight, the charging of the e-plane is expected to take place six times per day during Summer, and five times per day during Winter for ambient temperatures above -20 °C as per [43], spaced by one-hour intervals when the e-plane is in use. However, note that four charging operations have been considered for the coldest Winter day assuming that the e-plane would fly after the ambient temperature goes above -20 °C. As per Fig. 3, note that the power supplied by the charger is reduced when the e-plane battery SOC reaches 90% and continues to decrease slowly as the SOC comes closer to 100%. Furthermore, the e-plane demand profile considers that the lowest SOC level for the e-plane battery would be 30% at touchdown. Thus, an energy supply of approximately 14 kWh is assumed for each charging process.

Uncertainties in RES and demand are considered in the MPC process detailed in Section 2.1 and using a rolling time horizon of $T = 24$ h, divided into uniform-duration intervals of $\Delta t = 15$ min each. Thus, the optimization process starts at $k = 0$, where the forecast for the next

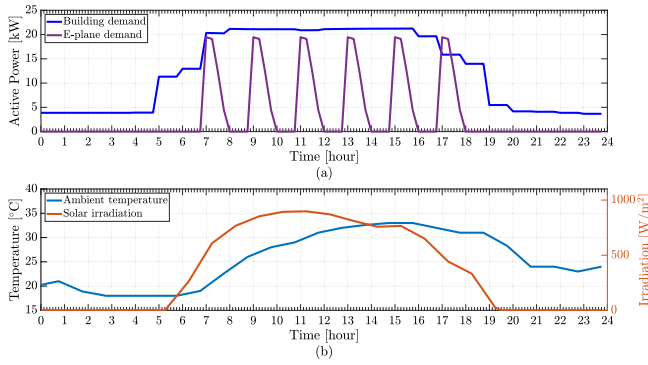


Fig. 4. (a) Electric demand and (b) environmental conditions for WWFC Hangar 7 for the hottest day in Summer.

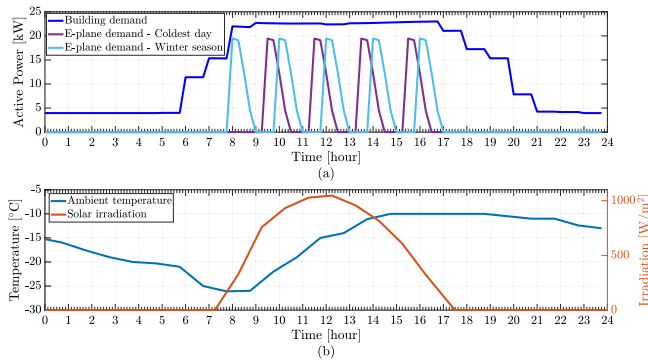


Fig. 5. (a) Electric demand and (b) environmental conditions for WWFC Hangar 7 for the coldest day in Winter.

24 h with 15 min intervals is obtained from a data set that contains the forecast for a two-day operation. The optimization problem is thus solved, with the solution for time k defining the equipment dispatch for the corresponding time intervals from 0 to 95, i.e., for 96 intervals. A linear increase in the forecast error over time is assumed, as per [44].

The power consumed by the e-plane charger along with the estimated building electric demand and the environmental conditions considered as EMS inputs for the hottest day in Summer and the coldest day in Winter, to showcase the performance of the proposed models under extreme conditions, are presented in Figs. 4 and 5, respectively. Observe that real data was used for representing the environmental conditions of such days considering the average hourly weather conditions in Ontario, Canada from 2007 to 2021 based on [45]. Furthermore, the predefined temperature limits are assumed to be a minimum of 21 °C during working hours, i.e., from 8 am to 9 pm, and 15 °C for the lower limit during the remaining hours, except for the planes' hangar that has a lower limit of 10 °C throughout the day. A maximum of 24 °C is assumed as the set point for all rooms, except for the planes' hangar, which has no cooling system. All simulations were performed using Gurobi solver on an AMD Ryzen 7 5700G processor, with a base speed of 3.80 GHz, resulting in an execution time of approximately six minutes and thirty seconds, which is well below the desired 15-minute EMS dispatch interval.

4.3. Simulation results

The simulation results for the operation of the WWFC microgrid EMS discussed next consider two pricing schemes: a Time of Use (TOU) Tariff [46], and a Fixed Tariff, which is the current pricing scheme adopted at the WWFC. The Fixed Tariff pricing scheme also considers CO2 emission intensity factors to account for the hangar impact on

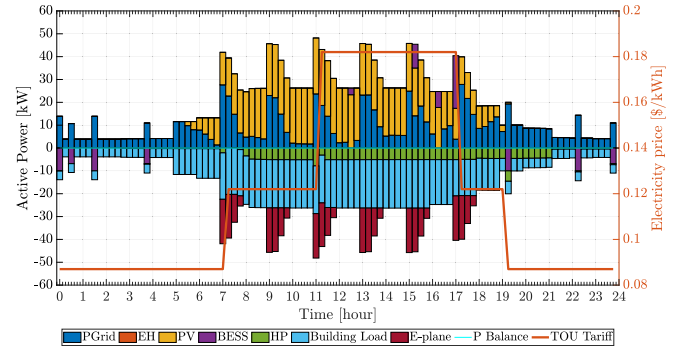


Fig. 6. Active power balance for the WWFC hangar microgrid under TOU Tariff for the hottest day in Summer.

emissions. This allows to realistically analyze the behavior of the microgrid's electric and thermal components in response to different price signals. Furthermore, for each of these schemes, the BESS SOC is represented with and without considering BESS degradation with a BESS replacement cost of 139 \$/kWh, based on [47]. Note that when degradation is not considered, the BESS operational cost is not included in the objective function but is quantified separately for comparison purposes. For the BESS operation, the initial BESS SOC is assumed to be 50%, as an average starting point, i.e., not too low nor too high, and the lower and upper limits are set to typical 20% and 90%, respectively, with a charging/discharging efficiency of 95%, as per [38].

4.3.1. TOU tariff

The daily operational costs for the microgrid under this pricing scheme, considering BESS degradation, are \$27.42 for Summer and \$33.17 for Winter. The active power balance in the microgrid for Summer and Winter resulting from executing the proposed EMS model is shown in Figs. 6 and 7, respectively. In both cases, it can be observed that the BESS operation follows an arbitrage behavior, i.e., the battery is charged when the price is lowest and discharged when it is highest. Note that for the coldest Winter day, there is significant PV generation due to the high solar irradiation levels, resulting in the BESS charging when the electricity price is not at its lowest to store excess power. Observe also that the TOU Tariff is different for Summer and Winter. The power consumed by the HPs and the EH varies depending on the thermal requirements of each room and also responds to price variations. In Summer, this is seen at 11 am when a pre-cooling operation occurs before the price increases. As expected, no operations of the EH are registered in this case. On the other hand, during Winter, the price response is evident at 7 am when the HPs and the EH operate to pre-heat the respective rooms. The BESS SOC for both Summer and Winter is portrayed in Figs. 8 and 9 with the BESS displaying a more intensive operation when the degradation function is not included.

The temperature variations inside the rooms of the WWFC hangar building, where it is assumed that a thermostat controls the operation of four HPs to independently maintain the temperature within predefined set limits for the hottest Summer day, are portrayed in Fig. 10; Fig. 11 illustrates the temperature of the planes' hangar, where the temperature is controlled by the EMS through an EH; and Fig. 12 shows the temperature in the rooms where the thermal supply from the HP depends on the thermal distribution factors μ_i , with the aim of avoiding drastic temperature changes which may lead to occupants' discomfort. Note that for the rooms where the set points are considered, the temperature remains between the defined limits at all times. For the planes' hangar, it can be seen that the temperature reaches high values since there are no cooling mechanisms. Furthermore, although the temperature constraints are not fully satisfied for the remaining rooms, observe that the temperature maintains adequate levels, indicating a proper allocation of thermal distribution weights for the HP operation.

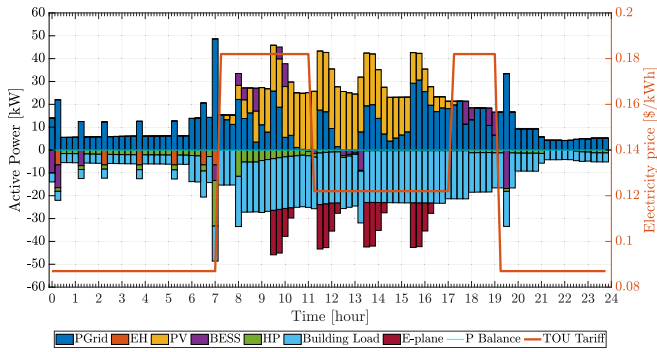


Fig. 7. Active power balance for the WWFC hangar microgrid under TOU Tariff for the coldest day in Winter.

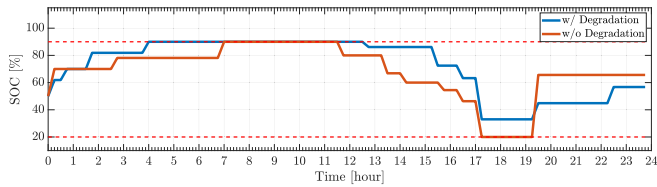


Fig. 8. SOC of the BESS under TOU Tariff for the hottest day in Summer.

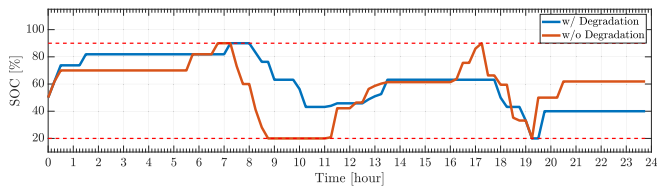


Fig. 9. SOC of the BESS under TOU Tariff for the coldest day in Winter.

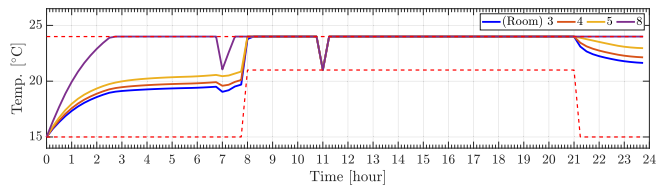


Fig. 10. Temperature inside Room 3, 4, 5, and 8 under TOU Tariff for the hottest day in Summer.

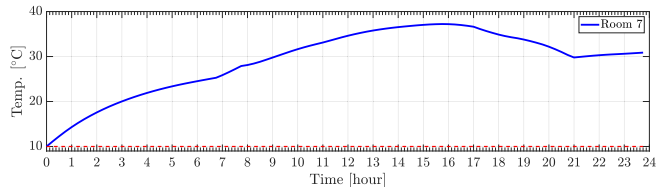


Fig. 11. Temperature inside Room 7 under TOU Tariff for the hottest day in Summer.

Finally, note that, besides Room 9, where the temperature is in close proximity to the set limits, the occupancy rate for the other rooms is quite low, with minimal impact on comfort levels.

For the Winter scenario, the temperature profiles inside the rooms with temperature control, the planes' hangar, and where the temperature is only monitored are portrayed in Figs. 13, 14, and 15, respectively. Similarly to the Summer case, the temperature where the set points are considered remains between the defined limits at all times. Note how at 7 am an increase in the room temperatures is

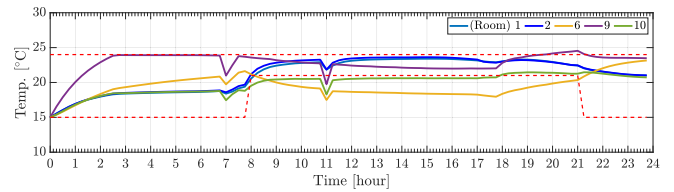


Fig. 12. Temperature inside Room 1, 2, 6, 9 and 10 under TOU Tariff for the hottest day in Summer.

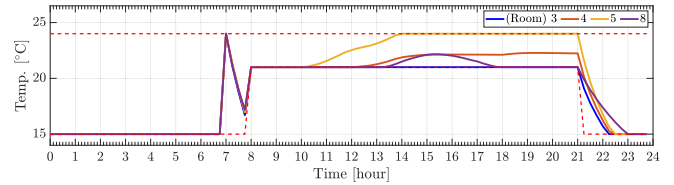


Fig. 13. Temperature inside Room 3, 4, 5, and 8 under TOU Tariff for the coldest day in Winter.

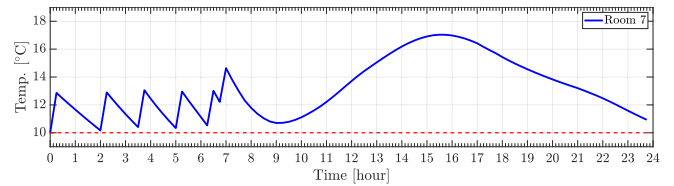


Fig. 14. Temperature inside Room 7 under TOU Tariff for the coldest day in Winter.

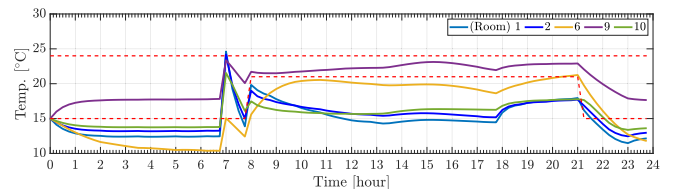


Fig. 15. Temperature inside Room 1, 2, 6, 9 and 10 under TOU Tariff for the coldest day in Winter.

registered due to pre-heating operations, and the temperature inside the planes' hangar is maintained above 10 °C through the operation of the EH. Observe that since the EH is controlled by the EMS, it also participates in pre-heating strategies to minimize operational costs. Finally, it can be seen for the remaining rooms that the temperature also maintains adequate levels, especially during working hours and where high occupancy is expected. Notably, due to the thermal distribution factors, a lower temperature in Rooms 1 and 2 is observed that prevents a larger temperature spike at 7 am.

In Winter, it is important to highlight that despite the cold ambient temperature there is a cooling requirement in Room 5 housing flight simulator 3 due to its high thermal power radiation. This is particularly relevant since, for instance, between 6 pm and 9 pm, when the HP controlling the temperature of this room is providing cooling power, the HP that controls the temperature inside the classrooms, i.e., Room 8, provides heating. Thus, a single HVAC system would not properly satisfy the thermal requirements.

4.3.2. Fixed tariff

In this section, a fixed electricity price of 0.142 \$/kWh, which is the current WWFC tariff, and different CO2 emission intensity factors for the hottest day in Summer and the coldest day in Winter are considered, as per [48]. Note that for this scenario, the CO2 emissions are linked to the power obtained from the main grid, as per (11), considering a social

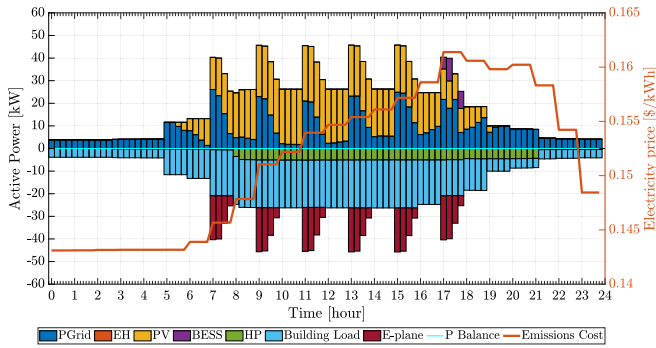


Fig. 16. Active power balance for the WWFC hangar microgrid under Fixed Tariff for the hottest day in Summer.

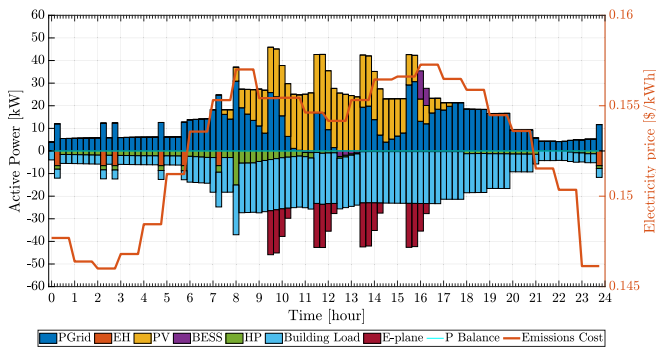


Fig. 17. Active power balance for the WWFC hangar microgrid under Fixed Tariff for the coldest day in Winter.

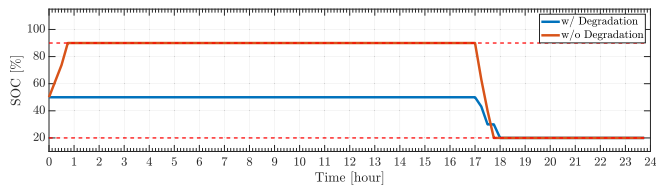


Fig. 18. SOC of the BESS under Fixed Tariff for the hottest day in Summer.

cost of carbon of 266 \$/tonne CO₂ [49]. The daily operational costs for the microgrid under the Fixed Tariff, considering BESS degradation, are \$31.79 for Summer and \$40.41 for Winter, with corresponding CO₂ emission costs of \$2.30 and \$3.12. The active power balance of the microgrid for Summer and Winter is portrayed in Figs. 16 and 17 for this case, along with the electricity price, including the equivalent social cost of carbon per kWh. Compared to the previous scenario, the BESS response to price signals is not as significant. However, the EH does respond with pre-heating operations. Furthermore, the BESS SOC is shown in Figs. 18 and 19. Note that in both cases the BESS presents a limited operation due to the similar electricity prices throughout the day.

In a similar fashion to the TOU Tariff scenario, Figs. 20, 21, and 22 illustrate the temperatures inside at the WWFC for the rooms where temperature is fully controlled, the planes' hangar, and the rooms where temperature is only monitored, for the Summer season. On the other hand, Figs. 23, 24, and 25 show the room temperatures for Winter. Note that, in both cases, the temperatures remain within the set limits where temperature control is enforced and maintain adequate levels in the remaining rooms, with neither pre-heating nor pre-cooling strategies being clearly observed, with the exception of the EH operation in the planes' hangar room.

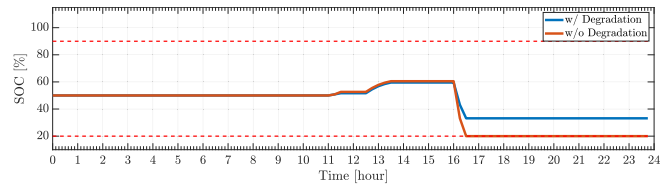


Fig. 19. SOC of the BESS under Fixed Tariff for the coldest day in Winter.

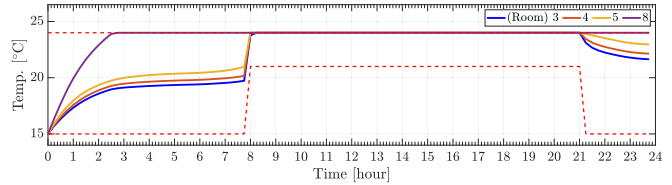


Fig. 20. Temperature inside Room 3, 4, 5 and 8 under Fixed Tariff for the hottest day in Summer.

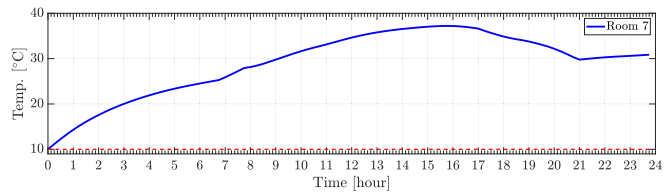


Fig. 21. Temperature inside Room 7 under Fixed Tariff for the hottest day in Summer.

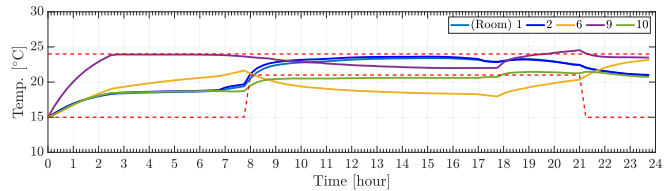


Fig. 22. Temperature inside Room 1, 2, 6, 9 and 10 under Fixed Tariff for the hottest day in Summer.

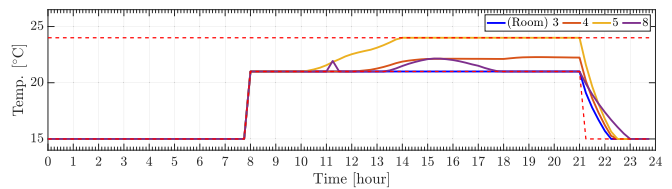


Fig. 23. Temperature inside Room 3, 4, 5 and 8 under Fixed Tariff for the coldest day in Winter.

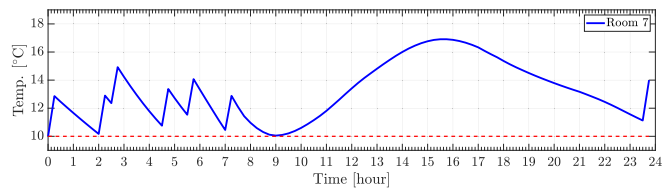


Fig. 24. Temperature inside Room 7 under Fixed Tariff for the coldest day in Winter.

4.3.3. Cost comparisons

Case Description

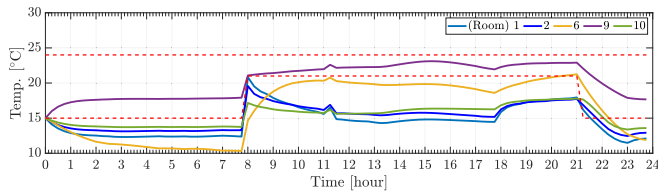


Fig. 25. Temperature inside Room 1, 2, 6, 9 and 10 under Fixed Tariff for the coldest day in Winter.

Table 5

Case studies.

Case	Description
Case 1	Microgrid without BESS degradation
Case 2	Microgrid with BESS degradation (proposed models)
Case 3	No microgrid deployment
Case 4	Microgrid with single-room, single-HP model

A comprehensive analysis and comparison are presented in this section of the operational costs of the thermo-electric system for the WWFC Hangar 7 using different models and operating modes. To this aim, four cases have been studied as follows:

- Case 1 considers the modeling of the WWFC microgrid including a multiple-room, multiple-HVAC system model, neglecting BESS degradation.
- Case 2 corresponds to the microgrid and EMS models proposed in this study, including BESS degradation.
- Case 3 assumes that there is no microgrid implementation, representing a “business-as-usual” operation with no BESS and no PV generation deployment.
- Case 4 assumes a single-room, single-HP model for the EMS, using a Thevenin equivalent approach to aggregate the heat gains from all rooms.

A summary of the different cases considered in the analysis is presented in Table 5. Note that these cases are evaluated under the two aforementioned pricing schemes, i.e., the TOU Tariff, and the Fixed Tariff with the addition of CO2 emission intensity factors.

TOU Tariff

The presented analysis includes an evaluation of the operation of the system during monthly average weekdays and weekends, with their corresponding TOU Tariff prices and environmental conditions, i.e., ambient temperature and solar irradiation, and electric consumption to determine a yearly cost of operation. Thus, Table 6 showcases the monthly average cost of operation of WWFC Hangar 7.

Fixed Tariff

This analysis evaluates the system’s operation considering operational costs from a CO2 emissions perspective using a monthly average of CO2 intensity factors and the Fixed Tariff pricing scheme along with the corresponding environmental conditions and electric demand from the building and the e-plane. Thus, Table 7 presents the monthly average cost associated with the CO2 produced from the operations at WWFC Hangar 7.

From a yearly perspective, as shown in Table 6, the incorporation of BESS degradation in the EMS model is evident in Case 2, since compared to Case 1, where degradation is not included, a cost reduction of around 1.1% is observed, which as expected, demonstrates that the inclusion of BESS degradation in short-term operation models is not significant. However, this issue is relevant in long-term BESS operation. Notably, Case 3, where the microgrid is not considered, incurs the highest costs, being almost 60% more expensive than Case 2. Furthermore, the incorporation of a multi-room building model with independent HVAC systems is highlighted, since Case 4 which considers a single-room, single-HP model, results in approximately

Table 6

Monthly operational costs at WWFC under different models and TOU tariff.

Scenario	Case 1 [\$]	Case 2 [\$]	Case 3 [\$]	Case 4 [\$]
Jan	1149.86	1136.56	1441.01	1310.26
Feb	1034.52	1028.48	1435.98	1111.68
Mar	886.31	859.32	1457.16	857.41
Apr	838.71	823.65	1511.27	797.02
May	820.58	812.26	1626.78	881.00
Jun	872.69	861.33	1675.50	932.14
Jul	793.02	778.31	1591.67	868.19
Aug	814.79	796.86	1589.17	892.89
Sep	1005.73	1010.06	1660.04	1057.96
Oct	1163.84	1159.45	1588.00	1128.76
Nov	1104.03	1097.79	1463.79	1058.28
Dec	1217.41	1208.59	1443.20	1289.11
Yearly	11701.50	11572.65	18483.57	12184.70

Table 7

Monthly costs of CO2 emissions at WWFC under different models and fixed tariff.

Scenario	Case 1 [\$]	Case 2 [\$]	Case 3 [\$]	Case 4 [\$]
Jan	76.81	76.81	97.08	87.97
Feb	87.22	87.22	122.58	97.35
Mar	75.26	75.26	122.97	76.45
Apr	27.12	27.11	47.90	26.28
May	30.00	30.37	55.80	31.07
Jun	46.10	46.53	84.13	49.39
Jul	99.53	99.53	189.55	109.89
Aug	82.69	82.69	156.37	89.95
Sep	58.60	58.93	92.79	60.48
Oct	48.41	49.20	65.67	47.23
Nov	63.15	64.28	83.50	63.00
Dec	88.37	88.37	105.79	96.10
Yearly	783.25	786.29	1224.12	835.15

5.3% increased operational costs compared to Case 2. On the other hand, as portrayed in Table 7, the operation of Case 3 is approximately 55.7% more expensive than Case 2 in terms of CO2 emissions. Thus, the proposed EMS model could achieve yearly savings of around \$438, which represents a reduction of 1.65 tonnes of CO2. Furthermore, compared to the single-room, single-HP model, Case 2 achieves an annual cost reduction of \$48.86, resulting in a reduction of 0.18 tonnes of CO2. Notably, Case 1, where BESS degradation is not included, incurs the lowest CO2-related costs due to reduced grid power consumption. However, compared to Case 2, the cost differences are minimal.

5. Conclusions

In this paper, the implementation of an EMS model for an airport hangar microgrid was discussed considering various thermal needs and resources and e-plane charging based on field measurements. A hangar building thermal model was developed, including the modeling of multiple HP-based HVAC systems for the provision of heating and cooling thermal power, and the impact produced by battery degradation processes. Moreover, an MPC approach was used to manage uncertainties in the forecast of demand and environmental conditions. The application of the proposed EMS model to an actual airport microgrid being deployed at the WWFC in Ontario, Canada, was presented, showcasing the need to model the specific characteristics of the microgrid components to properly assess the expected energy consumption and temperature control inside the different building areas, based on the electric equipment, occupancy patterns, and heat transfer processes. Thus, to study the performance of the developed EMS model, two pricing schemes were considered, namely the TOU Tariff and a Fixed Tariff with CO2 emission intensity factors. The results demonstrate the relevance of properly modeling the building’s multiple zones and

thermal systems for adequate temperature control in different rooms and optimal microgrid operations, compared to a conventional single-room building thermal model with a single HP and also highlight the importance of deploying a microgrid at the WWFC. Thus, it is shown that the proposed microgrid model and its EMS can bring significant benefits to the WWFC in terms of operational costs and CO₂ emissions while capitalizing on the available solar resources with PV systems and BESS.

CRedit authorship contribution statement

Pablo Verdugo: Writing – original draft, Visualization, Validation, Software, Methodology, Investigation, Formal analysis, Data curation, Conceptualization. **Claudio Cañizares:** Writing – review & editing, Validation, Supervision, Resources, Project administration, Funding acquisition, Conceptualization. **Mehrdad Pirnia:** Writing – review & editing, Validation, Supervision, Project administration, Funding acquisition, Data curation, Conceptualization.

Funding

This work has been supported by the Natural Sciences and Engineering Research Council of Canada (NSERC).

Declaration of competing interest

The authors declare that they have no known competing financial interests or personal relationships that could have appeared to influence the work reported in this paper.

Acknowledgment

We thank our colleagues from the University of Waterloo and the Waterloo Wellington Flight Centre that greatly contributed to the elaboration of this work with their expertise and the provision of data.

Data availability

Data will be made available on request.

References

- [1] Harland K, Gibson S, Dion J, Gajudhur N, Mifflin K. Heat exchange: How today's policies will drive or delay Canada's transition to clean, reliable heat for buildings. Tech. rep., Canadian Climate Institute; 2024.
- [2] Hannula I, Menendez JB, Bosoni T, Bressers A, Briens F, Connelly E, et al. The role of e-fuels in decarbonising transport. Tech. rep., International Energy Agency; 2024.
- [3] Canada's aviation climate action plan. Tech. rep., Transport Canada; 2022.
- [4] Wang Y, Li Y, Cao Y, Shahidehpour M, Jiang L, Long Y, et al. Optimal operation strategy for multi-energy microgrid participating in auxiliary service. *IEEE Trans Smart Grid* 2023;14(5):3523–34.
- [5] Masrur H, Shafie-Khah M, Hossain MJ, Senjyu T. Multi-Energy Microgrids Incorporating EV Integration: Optimal Design and Resilient Operation. *IEEE Trans Smart Grid* 2022;13(5):3508–18.
- [6] Li Z, Wu L, Xu Y, Moazeni S, Tang Z. Multi-stage real-time operation of a multi-energy microgrid with electrical and thermal energy storage assets: A data-driven MPC-adp approach. *IEEE Trans Smart Grid* 2022;13(1):213–26.
- [7] Ahmadi SE, Marzband M, Ikpehai A, Abusorrah A. Optimal stochastic scheduling of plug-in electric vehicles as mobile energy storage systems for resilience enhancement of multi-agent multi-energy networked microgrids. *J Energy Storage* 2022;55:105566.
- [8] Li Z, Xu Y. Optimal coordinated energy dispatch of a multi-energy microgrid in grid-connected and islanded modes. *Appl Energy* 2018;210:974–86.
- [9] Moretti L, Martelli E, Manzolini G. An efficient robust optimization model for the unit commitment and dispatch of multi-energy systems and microgrids. *Appl Energy* 2020;261:113859.
- [10] Emrani-Rahaghi P, Hashemi-Dezaki H, Ketabi A. Efficient voltage control of low voltage distribution networks using integrated optimized energy management of networked residential multi-energy microgrids. *Appl Energy* 2023;349:121391.
- [11] Anvari-Moghaddam A, Rahimi-Kian A, Mirian MS, Guerrero JM. A multi-agent based energy management solution for integrated buildings and microgrid system. *Appl Energy* 2017;203:41–56.
- [12] Liu G, Jiang T, Ollis TB, Zhang X, Tomsovic K. Distributed energy management for community microgrids considering network operational constraints and building thermal dynamics. *Appl Energy* 2019;239:83–95.
- [13] Violante W, Cañizares CA, Trovato MA, Forte G. An energy management system for isolated microgrids with thermal energy resources. *IEEE Trans Smart Grid* 2020;11(4):2880–91.
- [14] Vasilij J, Jakus D, Sarajcev P. Robust nonlinear economic MPC based management of a multi energy microgrid. *IEEE Trans Energy Convers* 2021;36(2):1528–36.
- [15] Zhang C, Xu Y, Li Z, Dong ZY. Robustly coordinated operation of a multi-energy microgrid with flexible electric and thermal loads. *IEEE Trans Smart Grid* 2019;10(3):2765–75.
- [16] Efkarpidis NA, Vomva SA, Christoforidis GC, Papagiannis GK. Optimal day-to-day scheduling of multiple energy assets in residential buildings equipped with variable-speed heat pumps. *Appl Energy* 2022;312:118702.
- [17] Liang X, Chen K, Chen S, Zhu X, Jin X, Du Z. IoT-based intelligent energy management system for optimal planning of HVAC devices in net-zero emissions PV-battery building considering demand compliance. *Energy Convers Manage* 2023;292:117369.
- [18] Li J, Jiang Z, Chen Z, Liu J, Cheng L. CuEMS: Deep reinforcement learning for community control of energy management systems in microgrids. *Energy Build* 2024;304:113865.
- [19] Gao G, Li J, Wen Y. Deepcomfort: Energy-efficient thermal comfort control in buildings via reinforcement learning. *IEEE Internet Things J* 2020;7(9):8472–84.
- [20] Calero I, Cañizares CA, Bhattacharya K, Baldick R. Duck-curve mitigation in power grids with high penetration of PV generation. *IEEE Trans Smart Grid* 2022;13(1):314–29.
- [21] Frahm M, Dengiz T, Zwickel P, Maaß H, Matthes J, Hagenmeyer V. Occupant-oriented demand response with multi-zone thermal building control. *Appl Energy* 2023;347:121454.
- [22] Ariwoola R, Kamalasan S. An integrated hybrid thermal dynamics model and energy aware optimization framework for grid-interactive residential building management. *IEEE Trans Ind Appl* 2023;59(2):2519–31.
- [23] Zeng C, Luo J, Yuan Y, Haghghat F. Energy, economic, and environmental (3E) performance assessment, comparison, and analysis of airport cargo terminal microgrid system under the islanded and grid-connected modes. *J Build Eng* 2024;82:108270.
- [24] Hou B, Bose S, Marla L, Haran K. Impact of aviation electrification on airports: Flight scheduling and charging. *IEEE Trans Intell Transp Syst* 2024;25(3):2342–54.
- [25] Bao D-W, Zhou J-Y, Zhang Z-Q, Chen Z, Kang D. Mixed fleet scheduling method for airport ground service vehicles under the trend of electrification. *J Air Transp Manag* 2023;108:102379.
- [26] Alruwaili M, Cipcigan L. Airport electrified ground support equipment for providing ancillary services to the grid. *Electr Power Syst Res* 2022;211:108242.
- [27] Guo Z, Zhang J, Zhang R, Zhang X. Aviation-to-grid flexibility through electric aircraft charging. *IEEE Trans Ind Inf* 2022;18(11):8149–59.
- [28] Guo Z, Li B, Taylor G, Zhang X. Infrastructure planning for airport microgrid integrated with electric aircraft and parking lot electric vehicles. *eTransportation* 2023;17:100257.
- [29] Kazemi M. Development principles of Pirkkala airport environment as microgrid solution [Master's thesis], Tampere University; 2023.
- [30] Ollas P, Sigarchian SG, Alfredsson H, Leijon J, Döhler JS, Aalhuizen C, et al. Evaluating the role of solar photovoltaic and battery storage in supporting electric aviation and vehicle infrastructure at visby airport. *Appl Energy* 2023;352:121946.
- [31] Xiang Y, Cai H, Liu J, Zhang X. Techno-economic design of energy systems for airport electrification: A hydrogen-solar-storage integrated microgrid solution. *Appl Energy* 2021;283:116374.
- [32] Zhao H, Xiang Y, Shen Y, Guo Y, Xue P, Sun W, et al. Resilience assessment of hydrogen-integrated energy system for airport electrification. *IEEE Trans Ind Appl* 2022;58(2):2812–24.
- [33] Olivares DE, Cañizares CA, Kazerani M. A centralized energy management system for isolated microgrids. *IEEE Trans Smart Grid* 2014;5(4):1864–75.
- [34] Córdova S, Cañizares C, Lorca A, Olivares DE. An energy management system with short-term fluctuation reserves and battery degradation for isolated microgrids. *IEEE Trans Smart Grid* 2021;12(6):4668–80.
- [35] Mendieta W, Cañizares CA. Primary frequency control in isolated microgrids using thermostatically controllable loads. *IEEE Trans Smart Grid* 2021;12(1):93–105.
- [36] Thermal environmental conditions for human occupancy. Standard, American Society of Heating, Refrigerating and Air-Conditioning Engineers; 2013.
- [37] Akbari E, Kapsis C. Waterloo wellington flight centre - Hangar 7 building energy modelling. Tech. rep., Waterloo, Ontario, CA: University of Waterloo; 2023.
- [38] Xu B, Zhao J, Zheng T, Litvinov E, Kirschen DS. Factoring the cycle aging cost of batteries participating in electricity markets. *IEEE Trans Power Syst* 2018;33(2):2248–59.

- [39] Thomas V. Internal Heat Gains (IHG). 2024, <https://energy-models.com/internal-heat-gains-ihg>. [Accessed 26 June 2024].
- [40] Ventilation and acceptable indoor air quality. Standard, American Society of Heating, Refrigerating and Air-Conditioning Engineers; 2022.
- [41] Velis Electro. 2024, <https://www.pipistrel-aircraft.com/products/velis-electro/>. [Accessed 1 July 2024].
- [42] Empowering Flight, Electrifying Tomorrow!. 2024, <https://electrify.uwaterloo.ca/>. [Accessed 28 August 2024].
- [43] Velis Electro Pilot's Operating Handbook. In: Handbook. Pipistrel; 2020.
- [44] Romero-Quete D, Cañizares CA. An affine arithmetic-based energy management system for isolated microgrids. *IEEE Trans Smart Grid* 2019;10(3):2989–98.
- [45] Climate.OneBuilding.Org. 2024, <https://climate.onebuilding.org/>. [Accessed 15 May 2024].
- [46] Electricity prices and costs. 2024, <https://www.hydroone.com/rates-and-billing/rates-and-charges/electricity-pricing-and-costs#TOU>. [Accessed 17 July 2024].
- [47] Catsaros O. Lithium-ion battery pack prices hit record low of \$139/kWh. *Tech. rep., bloombergNEF*; 2023.
- [48] Energy insight, carbon emissions. 2024, <https://live.gridwatch.ca/carbon-emissions.html/>. [Accessed: 23 July 2024].
- [49] Social cost of greenhouse gas emissions. *Tech. rep., Government of Canada*; 2023.